NUMERICAL STUDY ON LOAD-SETTLEMENT RELATIONSHIPS OF SHALLOW FOUNDATION UNDER EXTREMELY LOW CONFINING PRESSURE

H. AKAGI[1] K. SATO[1] AND T. KIRIYAMA[2]

[1] Waseda University, Department of Civil and Environmental Engineering
58-205, 3-4-1, Ohkubo, Shinju-ku, Tokyo, 169-8555, Japan
e-mail: akagi@waseda.jp, web page: http://www.f.waseda.jp/akagi/index_e.html

[2] Shimizu Corporation, Institute of Technology
3-4-17, Etchujima, Koto-ku, Tokyo, 135-0044, Japan
e-mail: kiriyama@shimz.co.jp, web page: https://www.shimz.co.jp/en/

Key words: Material Point Method, Shallow Foundation, Large Deformation

Abstract. In order to investigate the ground behavior under shallow foundation with extremely low confining pressure, numerical analysis has been performed using the Material Point Method. Material Point Method is one of particle-based methods but it still uses numerical grid. It has been applied to many problems of geomaterial since it was proposed for the first time. The authors focus on the robustness of the method under large deformation problem and applied it to the shallow foundation problem of geomaterial. In this paper, the formulation and implementation of Material Point Method are described, followed by verification and validation for the implemented code. Then, the parametric investigations on ground behavior under shallow foundation have been carried out.

1 INTRODUCTION

Foundation stone has been employed for thousands of years to support historical structures. The foundation stone support system is basically composed of a base ground, foundation stones, and an upper structure. Self-weight of an upper structure is transferred from structural columns to a base ground through foundation stones. In this support system, main purpose of foundation stones is to distribute a concentrated column force in a foundation stone body, relaxing stress concentration at the bottom of columns.

In this support system, foundation stones often penetrate into a base ground once they are undergoing additional external forces such as earthquakes because surface grounds around foundation stones don't have enough bearing capacity due to an extremely low confining pressure condition. Conventional bearing capacity theory is employed when it can be regarded as it be under the small deformation condition whereas it becomes difficult to evaluate bearing capacities and to predict settlements under the large deformation condition such in case of foundation stones. The conventional method is based on an assumption of rigid-plastic behaviour and it focuses on a bearing capacity at an ultimate state. Therefore, the same approach cannot be applied to the case under large deformation conditions, which include geometrical nonlinearity.

In order to assess the support system behaviour under extremely low confining pressure,

experimental and numerical study are the main options to be chosen. Experimental testing is performed and reported in the companion papers by the same authors, demonstrating that a load-settlement relationship under large deformation condition shows much higher bearing capacity than the case of small deformation condition, demanding incremental external force for a footing to settle. In this paper, the demonstration of the applicability of numerical simulation is to be focused, employing a particle-based numerical method, which have been applied to geomaterial literally [1]. A shallow foundation model is set up numerically, in which footing foundation is modelled as elastic and a base ground is modelled as elasto-plastic material with Mohr-Coulomb failure criteria. Then, the support system behaviour is assessed by comparing the experimental results with the simulation results.

From comparison between experimental and numerical results, the load-settlement relationship by both methods gives a good agreement to each other, meaning particle-based numerical method is capable of simulating the behaviour of the support system under extremely low confining pressure.

2 MATERIAL POINT METHOD

The Material Point Method (MPM), which is originally proposed by Sulsky et al. [1], is a derivative of Particle-In-Cell (PIC) [2], in which a particle has all physical quantities but the equation of motion is solved at grid point. PIC is formulated based on for Fluid Mechanics while MPM is based on Solid Mechanics. Physical quantities at material point are transferred to grid point by using interpolation functions. After equation of motion is solved at grid point, the solution is going back to material point by using interpolation function again. The transferring of physical quantities by using interpolation function is repeated at every numerical step. The first Material Point Method, call original MPM in this paper, uses 4-node shape function for the interpolation function in two-dimensional problems. However, the numerical oscillation occurs when material point crosses the numerical grid because the derivative of the shape function flips its value from plus to minus or vice versa. In order to overcome the numerical oscillation, Generalized Interpolation Material Point (GIMP) method is proposed by Bardenhagen and Kober [3], in which the interpolation function is averaged over its control domain. Hereafter, many interpolation functions have been reported on Material Point Method while most of them are derivative of GIMP method. In this section, the formulation of original MPM and GIMP method are described. The simulation of verification and validation are performed with both original MPM and GIMP method.

2.1 Formulation of Material Point Method

In the following equations, superscript k is the time step and subscript g and p are the physical quantities at the grid point and material point, respectively. The grid point mass is extrapolated from the material point mass as

$$m_g^k = \sum_{i=1}^{n_p} m_{p,i} S_{p,i} \tag{1}$$

in whici m_g, m_p, S_p, n_p are the mass of the grid point, the mass at the material point, the interpolation function value at the material point, and the number of material points in the

reference cell, respectively. The grid point internal force is calculated by integrating the stresses of the reference material points as

$$f_g^{int,k} = -\sum_{i=1}^{n_p} \frac{m_{p,i}^k}{\rho_{p,i}^k} G_{p,i}^T \sigma_{p,i}^k \tag{2}$$

in which f_g^{int}, ρ_p, G_p, σ_p, are the grid point internal force, the density of material point, interpolation function derivative value at the material point and the stress of the material point, respectively. The grid point external force is calculated as

$$f_g^{ext,k} = m_g^k \cdot g^k \tag{3}$$

in which f_g^{ext} is the grid point external force and g is the gravitational acceleration. Eqs. (1)-(3) yields the equation of motion in each direction(x and y) of the grid point as

$$a_g^k = \frac{1}{m_g^k}\left(f_g^{int,k} + f_g^{ext,k}\right) \tag{4}$$

in which a_g is the acceleration of the grid point. The material point coordinates are updated as

$$x^{k+1} = x^k + \Delta t \cdot \sum_{i=1}^{n_g} v_{g,i}^k S_{p,i}^k \tag{5}$$

in which x, v, Δt, n_g are the material points coordinates, the grid point velocity, the incremental time, and the number of grid points in the cell to which the reference material point belongs. The material point displacement(u), acceleration(a_p) and velocity(v_p) are updated as

$$u^{k+1} = u^k + \Delta t \cdot \sum_{i=1}^{n_g} v_{g,i}^k S_{p,i}^k \tag{6}$$

$$a_p^k = \sum_{i=1}^{n_g} a_{g,i}^k S_{p,i}^k \tag{7}$$

$$v_p^{k+1} = v_p^k + \Delta t \cdot a_p^k \tag{8}$$

The grid point velocity(v_g) is updated as

$$v_g^k = \sum_{i=1}^{n_p} \frac{S_{p,i} m_{p,i}}{m_g^k} v_p^k \tag{9}$$

The material point strains(ε_p) are updated as

$$\Delta\varepsilon_p^k = \frac{\Delta t}{2} \cdot \sum_{i=1}^{n_p} \left(G_{p,i} v_g^k + \left(G_{p,i} v_g^k\right)^T\right) \tag{10a}$$

$$\varepsilon_p^{k+1} = \varepsilon_p^k + \Delta\varepsilon_p^k \tag{10b}$$

in which $\Delta\varepsilon_p$ is the incremental strain during a time step (Δt). The material point stresses are updated as

$$\Delta\sigma_p^k = K \cdot \Delta\varepsilon_p^k \tag{11a}$$

$$\sigma_p^{k+1} = \sigma_p^k + \Delta\sigma_p^k \tag{11b}$$

in which $\Delta\sigma$ is the incremental stress during time step Δt. As seen in Eq. (10), the stress and strain objectivities are not satisfied. They are assumed to increase linearly during time step Δt, which is set to be very small (e.g., $1.0\text{x}10^{-5}$(s)). The volume (*Volume*) and density (ρ) of the material point are updated as

$$Volume^{k+1} = Volume^k \cdot (1 + \Delta\varepsilon_v^k) \tag{12}$$

$$\rho^{k+1} = \frac{\rho^k}{\left(1 + \Delta\varepsilon_v^k\right)} \tag{13}$$

When using GIMP method, in which the particle control domain is considered, the widths of the material points(l_p) are updated as

$$l_p^{k+1} = l_p^k \cdot \left(1 + \Delta\varepsilon_i^k\right) \tag{14}$$

The widths of material points are often not updated for practical reason. Then, the method, which updates the widths, is called contigous particle GIMP (cpGIMP) method whereas the method, which does not update the widths, is called unchanged/uniform GIMP (uGIMP) method.

The numerical procedure from Eq.(1) to Eq.(13) corresponds to one cycle of the MPM algorithm, and the incremental time is Δt. To solve time interval t, the procedure above cycles for the number of time steps, which becomes $t/\Delta t$ times.

3 VERIFICATION AND VALIDATION OF THE METHOD

In order to confirm the integrity of the implemented code, the verification and validation for the code is performed. The importance of the verification and validation (V&V) has been increased as the numerical simulation is more applied in practical engineering use. In this section, the implementations of GIMP method are verified by using the theoretical solution and validated by comparison with the experimental result.

3.1 Verification using one dimensional solution under large deformation

For the investigation of shallow foundation problem under large deformation, the total stress formulation is employed. Then, the formulation is verified by comparing the numerical solution with the total stress theoretical solution under large deformation condition. Zhang et al. [4] proposed the theoretical solution for one-dimensional column under gravitational force by assuming that the potential energy is kept constant based on the finite deformation theory. Theoretical stress and displacement of Zhang's 1D column are described as follows.

$$\sigma(x) = \sigma(0)\frac{(1 - x/h_0) + \kappa(x/h_0)}{1 - \kappa(1-\kappa)(x/h_0)}, \text{where } \kappa = \frac{\sigma(0)}{2E} \tag{33}$$

$$X - x = \kappa[2 - \kappa - (1-\kappa)\, x/h_0]/[1 - \kappa(1-\kappa)/(x/h_0)] \tag{34}$$

in which X and x are the initial and the current coordinates from the bottom of column, respectively. h_0 is the length of the column. $\sigma(x)$ is the stress at the coordinate of x. E is Young's Modulus.

For the verification problem, the numerical model for the one-dimensional column is prepared. 50 particles are lined with the length of 1 m, meaning each particle has 2 cm wide control domain. Column is discretized with 50 cells of numerical grid, in which one particle is arranged in each cell. Young's modulus and unit weight of particles are 10,000 kPa and 9.8 kN/m^3, respectively. The gravitational force is applied to the column incrementally with the damping coefficient [5] of 0.8 in order to obtain the quasi-static equilibrium solution. Figure 1 shows the comparison between numerical results and theoretical solutions. The numerical solutions give a good agreement to the theoretical one under 1G gravitational force (Fig. 1(a)). Original MPM begins to show the oscillation under 10G condition while uGIMP and cpGIMP method still give a good agreement to the theoretical one (Fig. 1(b)). Under 20G condition, uGIMP begins to show the oscillation, which becomes much more under 50G condition while cpGIMP still shows a good agreement to the theoretical solution (Fig. 1(c), (d)). The uGIMP solution is oscillate around the theoretical one. In the elastic problem the solution by uGIMP method may acceptable in case that only deformation is focused. However, in case of nonlinear problem, only cpGIMP solution is applicable because unexpected deformation occurs if particles reach yield surface during their stress oscillation.

3.2 Validation by comparing numerical result with experimental results

In order to validate the numerical simulation method, numerical results are compared with the experimental results of load-settlement relationship and strain distribution in the ground. The experiments are performed in physical simulation of shallow foundation, in which the ground and the foundation are modeled by aluminum bar and brass block as a rigid footing, respectively. The footing is controlled by displacement, penetrating into the ground while the load and the displacement are monitored by load-cell and displacement sensor, both of which are attached to the footing. The digital camera, which is located besides the physical model, captures snap shots of deformed ground during the loading. By using Particle Image Velocimetry (PIV) technique, displacement and maximum shear strain distribution inside the ground are visualized at every 5 mm penetration.

The numerical procedure, which simulates the experiment, is described below. Fig. 2 shows the initial configuration of the model and boundary condition. The numerical model is a half model by using the geometrical symmetry, in which the left side is the symmetric center. 4 particles are arranged regularly in one cell. The spacial resolution of the numerical model is defined as 5 mm, which is the same as the resolution of image analysis (PIV) in the experiment, which enables the direct comparison of strain. Table 1 and 2 show material properties and numerical conditions, respectively. During the simulation, the density of the loading block is changed gradually, which generates the increase in contact force and induce the ground

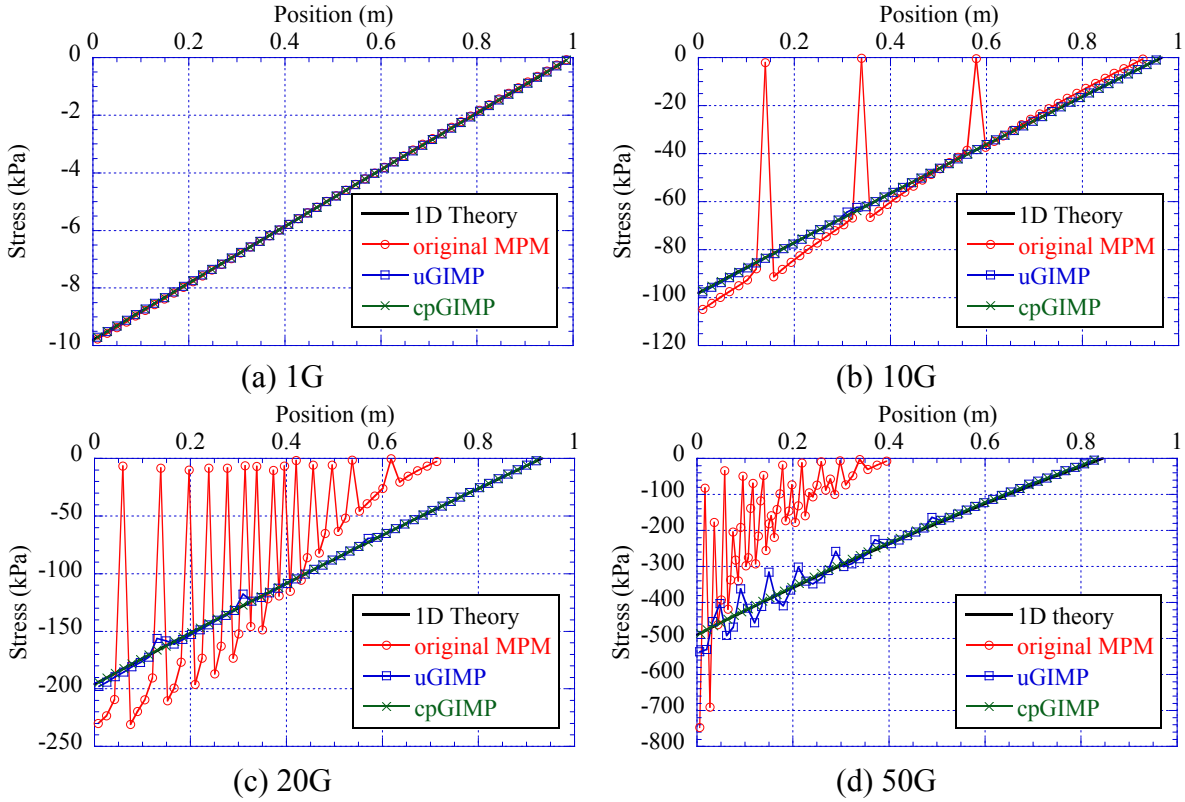

Figure 1. Comparison between numerical result and theoretical solution

deformation. The numerical load-settlement relationship is calculated by monitoring both the self-weight and the penetration of the loading block. Fig. 3 shows the load-settlement relationship obtained from both experiment and numerical simulation, which give a quite similar relationship. Fig. 4 shows the vertical displacement of the ground at the footing penetration of 5, 15, and 25 mm. The vertical displacements by both experiments and simulation also give a good agreement to each other. These comparison of load-settlement relationship and

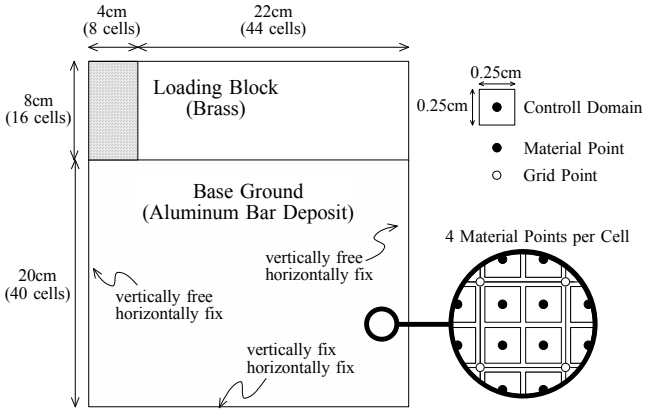

Figure 2. Numerical model of shallow foundation experiments

Table 1. material properties

E (kPa)	ν	ρ (g/cm^3)	ϕ (deg)	c (kPa)
1000	0.3	2.43	20	0

Table 2. numerical condition

Items	Values
Particles Per Cell	4
Dimensions(H x W)	0.26 m x 0.28 m
Width of cell	0.005 m
Time increment	0.000015
Damping factor	0.8
Number of Particles	
Ground	8,320
Footing	512

deformations inside the ground validate that the simulation result are evaluated as applicable for shallow foundation problems.

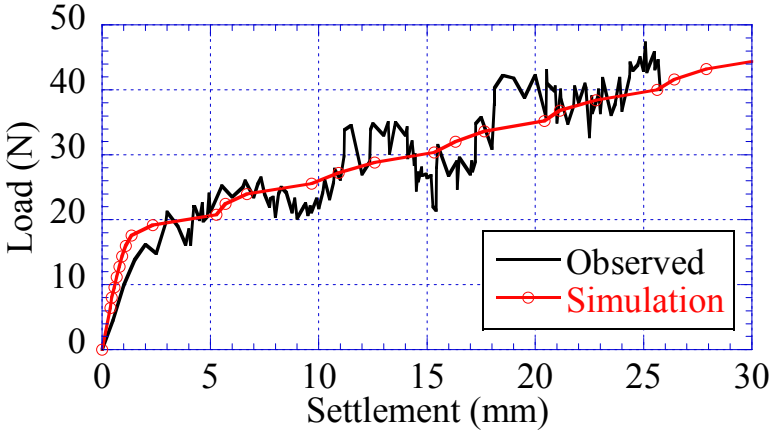

Figure 3. Comparison of load-displacement relationship between experimental and numerical results

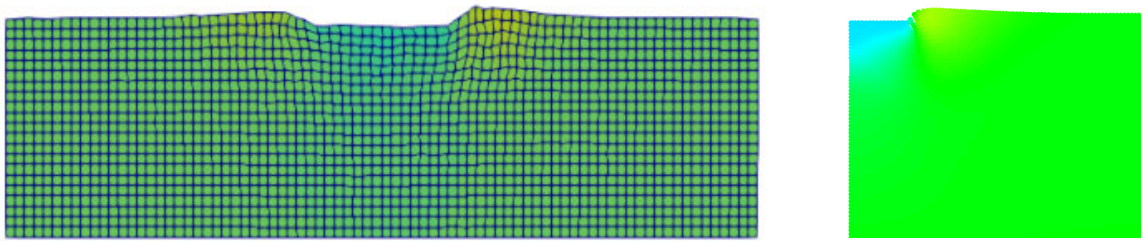

(i) observed (ii) simulation

(a) settlement=5mm

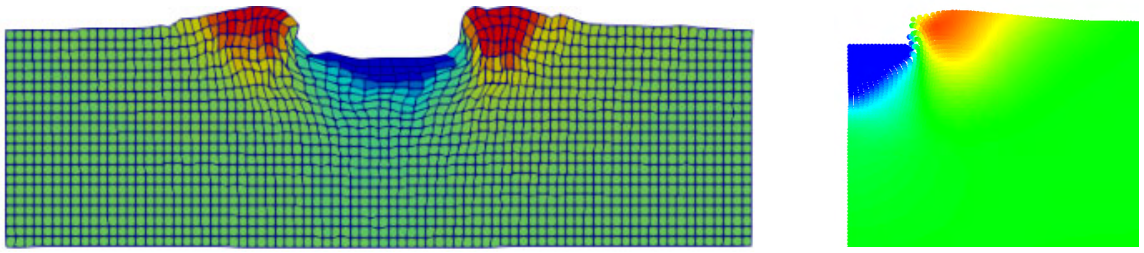

(i) observed (ii) simulation

(b) settlement=15mm

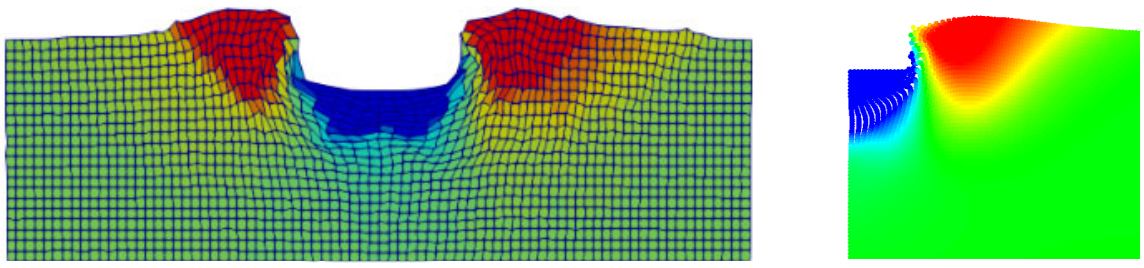

(i) observed (ii) simulation

(c) settlement=25mm

Figure 4. Comparison of settlement between experimental and numerical results

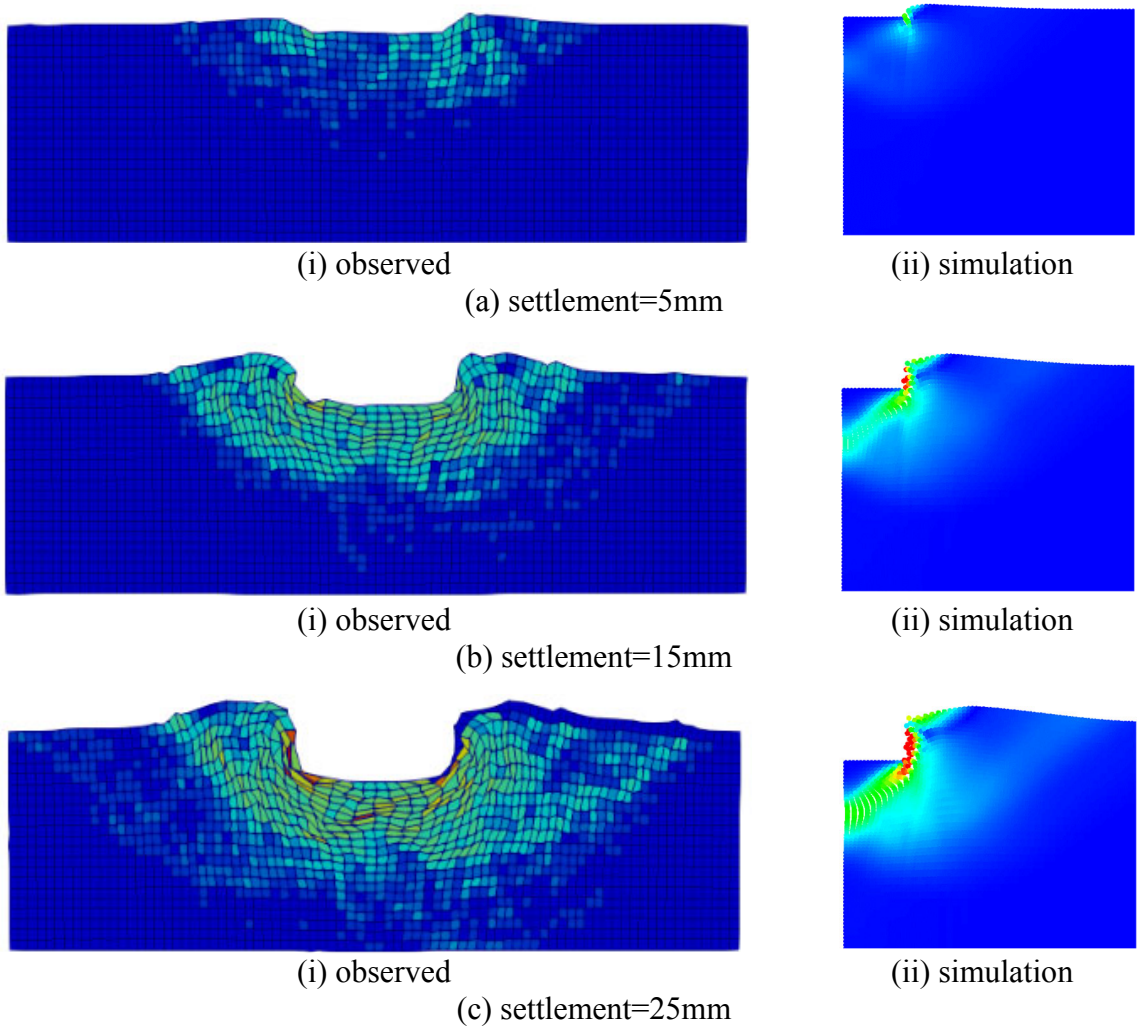

(i) observed (ii) simulation

(a) settlement=5mm

(i) observed (ii) simulation

(b) settlement=15mm

(i) observed (ii) simulation

(c) settlement=25mm

Figure 5. Comparison of maximum shear strain between experimental and numerical results

4 SHALLOW FOUNDATION BEHAVIOR UNDER LOW CONFINING PRESSURE

In order to understand the ground behavior under shallow foundation, parametric study using Material Point Method is performed. The same numerical model in previous section is employed with different material strength, which is changed as frictional or cohesive material to make it simple to understand the ground behavior. Table 3 shows material strength in the simulation. Cases from 1 to 3 are for understanding the behavior with frictional soil and cases from 4 to 6 are for cohesive soil. The load-settlement relationships and deformation inside the ground are obtained from the series of simulations, which are explained below.

4.1 Ground behavior of frictional soil under shallow foundation

Fig. 6 shows the load-settlement relationship obtained from soil condition with three different internal frictional angles of 15, 20 and 25(degree). The curves in Fig. 6 indicate two

Table 3. Material strength

Case	E (kPa)	ρ (kN/m^3)	Poisson's ratio ν	ϕ (deg)	c (kPa)
1	1000	20.0	0.3	15.0	0.0
2				20.0	0.0
3				25.0	0
4			0.4	0.0	0.5
5				0.0	1.0
6				0.0	2.0

phases. The first phase shows hardening behavior with different initial stiffness, which is seen in Fig. 6. The second phase shows the ultimate behavior, which is corresponding to the practical bearing capacity. It is quite difficult for the practical use to determine the initial stiffness every time only strength parameter changes. In the previous chapter, the initial stiffness has been determined by calibrating the material properties. It is also difficult to determine soil stiffness without any geotechnical investigation prior to the assessment. Then, geotechnical investigation is strongly recommended before assessing the frictional soil behaviors. Fig. 7 shows the total displacement and maximum shear strain, in which the punching type failure mechanism is observed in the first phase (Fig. 7(a)-(i),(b)-(i)) while the Terzaghi's bearing capacity theory

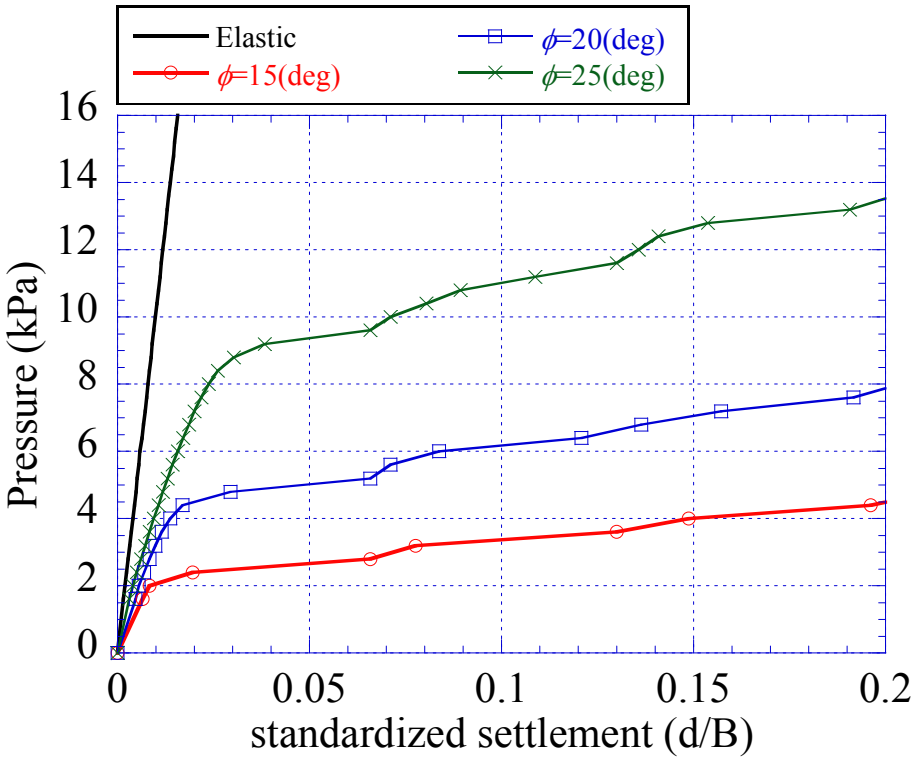

Figure 6. Load-settlement relationship of the frictional material ground

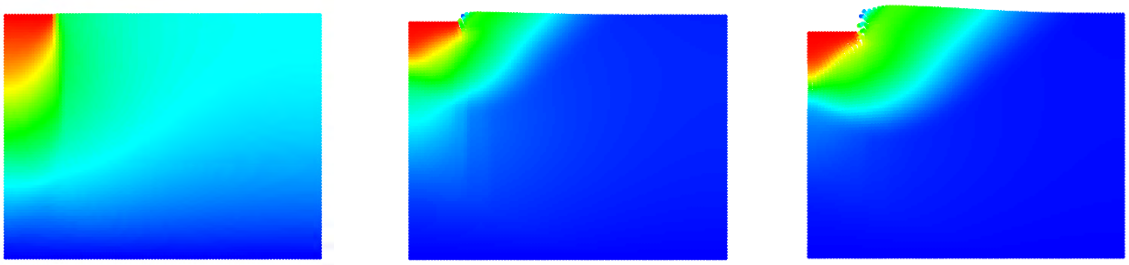

(i) Pressure=4(kPa) (ii) Pressure=10(kPa) (iii) Pressure=13.2(kPa)

(a) Total displacement

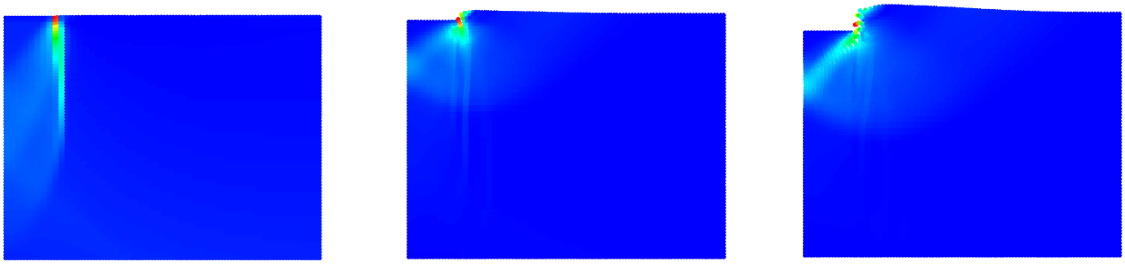

(i) Pressure=4(kPa) (ii) Pressure=10(kPa) (iii) Pressure=13.2(kPa)

(b) Maximum shear strain

Figure 7. Deformation inside the frictional material ground (Case3: ϕ=25(deg))

type failure mechanism is observed in the second phase (Fig. 7(a)-(ii),(iii),(b)-(ii),(iii)). The bearing capacities in Fig. 7 exceed the Terzaghi's theory. This is mainly due to the embedded effect under large deformation condition. In the theory, the embedded effect act only as an additional resistance but it extends the sliding line under large deformation, resulting in the more effect on the bearing capacity than the Terzaghi's theory.

4.2 Ground behavior of cohesive soil under shallow foundation

Fig.11 shows the load-settlement relationship obtained from soil condition with three different cohesions of 1.0, 2.0 and 3.0(kPa). The curves in Fig.11 indicate three phases. The first phase shows elastic behaviors, in which all the material shows the same line. The second phase shows the hardening behavior, which is a transient phase from elastic status to the ultimate status. The third phase shows the ultimate behavior, which is corresponding to the practical bearing capacity. Fig. 8 shows the total displacement and maximum shear strain, in which the elastic behavior is observed in the first phase, forming the displacement bubble (Fig. 8(a)-(i),(b)-(i)), followed by the second phase in which the punching type failure mechanism is observed(Fig. 8(a)-(ii),(b)-(ii)), and the third phase in which the Terzaghi's bearing capacity theory type failure mechanism is observed(Fig. 8(a)-(iii),(b)-(iii)). The bearing capacities in Fig.11 exceed the Terzaghi's theory. As seen in the result of frictional material, this is also due to the embedded effect under large deformation condition. The importance of considering the geometrical nonlinearity is recognized from the results.

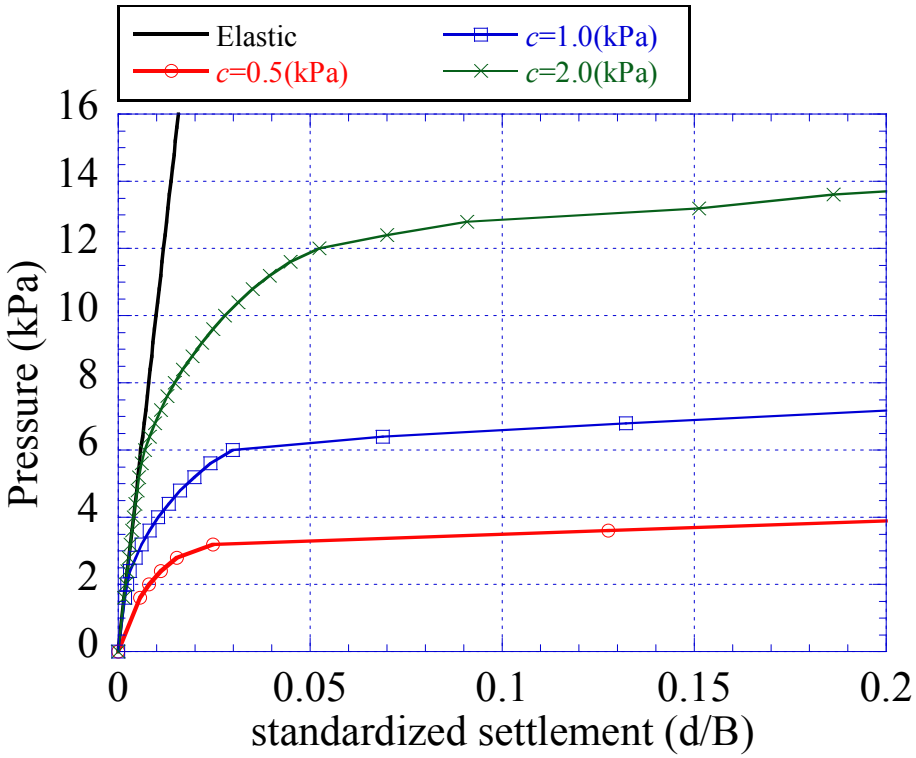

Figure 8. Load-settlement relationship of the cohesive material ground

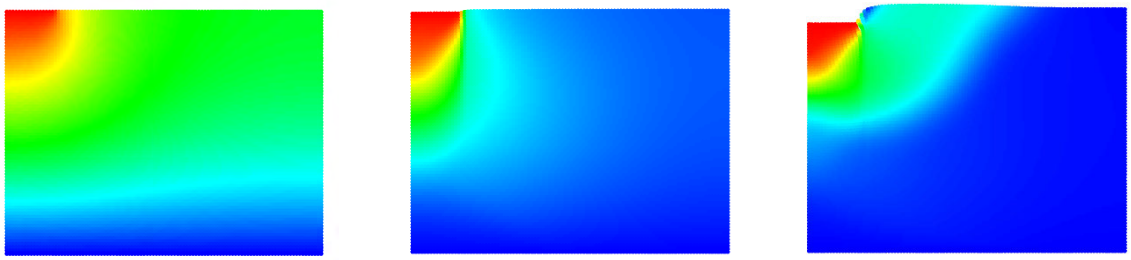

(i) Pressure=4(kPa) (ii) Pressure=10(kPa) (iii) Pressure=13.2(kPa)

(a) Total displacement

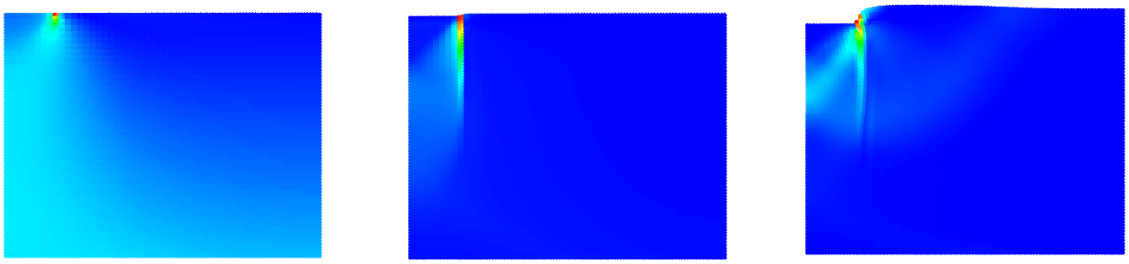

(i) Pressure=4(kPa) (ii) Pressure=10(kPa) (iii) Pressure=13.2(kPa)

(b) Maximum shear strain

Figure 9. Deformation inside the cohesive material ground (Case6:c=2(kPa))

5 CONCLUTION

In this paper, the formulation, verification and validation of the Material Point Method are reviewed, in which the difference of the formulation are scribed and the oscillation of the original MPM are demonstrated while the GIMP does not show any numerical oscillation. In the validation simulation, the numerical simulation results are compared with the experimental results. The load-settlement relationship and the deformation of the ground obtained from both simulation and experiment shows a good agreement to each other, showing the validity of the numerical method. After that, the parametric studies on the ground behavior are reported, in which ground behavior with different material strength are simulated. The ground behavior with frictional material shows the load-settlement curve with two phases, which are the foundation punching behavior in the first phase and Terzaghi's type sliding behavior in the second phase. The ground behavior with cohesive material shows the load-settlement curve with three phases, which are the elastic response in the first phase, followed by the punching and Terzaghi's type sliding in second and third phase respectively.

REFERENCES

[1] D. Sulsky, Z. Chen and H.L. Schreyer, (1994). A particle method for history-dependent materials, Computer Methods in Applied Mechanics and Engineering, 118, 179-196.

[2] Harlow, F.H., (1956). A Machine Calculation Method for Hydro-dynamic Problems. Los Alamos Scientific Laboratory re-port LAMS.

[3] Bardenhagen, S. G. & Kober, E. M. (2004). The generalized interpolation material point method, Computer Modeling in Engineering and Science 5(6), 447-495.

[4] Zhang, D.Z., Ma, X. and Giguere, P.T., (2011). Material point method enhanced by modified gradient of shape function, Journal of Computational Physics, Vol.230, pp.6379-6398.

[5] Cundall, P. A. (1987). Distinct element models of rock and soil structure, analytical and computational methods in engineering rock mechanics, Ch.4, 129-163. E.T. Brown, ed. London : Allen & Unwin.